Available online at www.sciencedirect.com
SCIENCE DIRECT®
ELSEVIER
Journal of Magnetism and Magnetic Materials 261 (2003) 210–221
journal of magnetism and magnetic materials
www.elsevier.com/locate/jmmm

Anisotropic properties of rare earth silver dibismites

C. Petrovic*, S.L. Bud'ko, J.D. Strand, P.C. Canfield

Ames Laboratory, Department of Physics and Astronomy, Iowa State University, Ames, IO 50011, USA

Received 30 September 2002

Abstract

We report measurements of structural, magnetic, thermal and transport properties of the newly synthesized rare earth silver dibismite series $RAgBi_2$ (R = La–Nd, Sm, Gd), grown via self-flux method. All of the compounds are metals, and those with magnetic ions exhibit long-range magnetic order at low temperatures, with the exception of $PrAgBi_2$. For the lightest rare earths the samples are of extremely high quality. For $LaAgBi_2$ de Haas van Alphen oscillations are found in remarkably small fields and high temperatures. The magnetic ground states for compounds that order magnetically appear to be antiferromagnetic, but with less local moment anisotropy than that seen in RBi_2. Anisotropic metamagnetism is observed for $CeAgBi_2$; however, no large magnetoresistance was observed in any of $RAgBi_2$, as opposed to either the $RAgSb_2$ or RSb_2 series. Magnetic ordering temperatures scale poorly with de Gennes scaling.

PACS: 75.30.G; 75.50; 75.60.E; 75.40

Keywords: Crystal growth; Magnetic anisotropy; Rare earth silver dibismites

1. Introduction

Rare earth silver diantimonides and structurally related rare earth diantimonides have been the concern of numerous studies [1–10]. In this work we present the results of structural, magnetic and transport studies on members of a new rare earth ternary series $RAgBi_2$ (R = La–Nd, Sm–Gd), which is isostructural with the $RAgSb_2$ series. The successful growth of single crystals allowed us to study magnetic anisotropy and its evolution with change of the rare earth ion. All $RAgBi_2$ compounds except $LaAgBi_2$ and $PrAgBi_2$ exhibit long-range magnetic order, but with less magnetic anisotropy than the isostructural $RAgSb_2$ or the structurally related RBi_2 and RSb_2 series [1,6,11]. On the other hand, de Haas van Alphen oscillations (dHvA) have been observed for $LaAgBi_2$ in $H < 70$ kOe and below the remarkably high $T < 40$ K, pointing to extremely light effective masses in its electronic structure. $RAgBi_2$ compounds with light rare earths have excellent crystal quality, inferred from small residual resistivities and high residual resistivity ratios (RRR's) as well as the dHvA results mentioned above. However, sample quality is quickly lost with substitution of heavier rare earths, with RRR's dropping from RRR = 25–65 for R = La–Pr to RRR = 2.5 for $GdAgBi_2$. No large magnetoresistances have been found in these compounds (even in $LaAgBi_2$),

*Corresponding author. Tel.: +515-294-3986; fax: +515-294-0689.
E-mail address: petrovic@bnl.gov (C. Petrovic).

0304-8853/03/$ - see front matter
doi:10.1016/S0304-8853(02)01476-2

implying smaller relaxation times than in the case of $RAgSb_2$ and RSb_2 [1,6].

2. Sample preparation and experimental techniques

Large single crystals of $RAgBi_2$ were grown from a ternary melt with an initial composition $R_{0.14}Ag_{0.14}Bi_{0.72}$ for R = (La, Ce, Nd, Sm) and $R_{0.045}Ag_{0.091}Bi_{0.864}$ for R = Gd. The elemental constituents were placed in an alumina crucible and sealed in a quartz ampoule in vacuum. The melt was heated up to 1100°C, quickly cooled to 1000°C, and then cooled to 400°C over a period of 130–160 h [12–14]. Once the ampoule reached the final temperature of 400°C the excess Bi was decanted. Crystals grew in the shape of malleable plates that were better formed than RBi_2 crystals and that could not be exfoliated [11]. The difference in structure and mechanical properties between $RAgBi_2$ and RBi_2 is due to silver atoms that provide additional bonding along the *c*-axis [1]. Powder X-ray diffraction was performed on all of the silver dibismites and the patterns were indexed in P4/nmm space group with a distribution of Miller indices similar to that for $RAgSb_2$, implying $ZrCuSi_2$ crystal structure type [1]. In addition, the Curie–Weiss analysis of the high-temperature susceptibility of the crystals (discussed below) also points to the $RAgBi_2$ stoichiometry. Due to sample malleability, diffraction peaks were rather broad and of small intensity. It introduced difficulty in refinement and a relatively large uncertainty in the magnitude of lattice parameters. A typical powder pattern ($NdAgBi_2$) is shown in Fig. 1. Strong reflections in the pattern are Bi flux (#) and Si standard (*). All other peaks are indexed to a tetragonal lattice with lattice constants $a = 4.51(2)$ Å, $c = 10.3(1)$ Å. As opposed to orthorhombic rare earth dibismites and diantimonides, rare earth silver dibismites and silver diantimonides are tetragonal, with the rare earth ion in a site with tetragonal point symmetry [1,15–17]. We estimate that the "*a*" lattice constant in the $RAgBi_2$ series decrease monotonically from R = La ($a = 4.60(1)$ Å) to R = Sm ($a = 4.44(4)$ Å), whereas the "*c*" lattice constant remains relatively unchanged ($c = 10.36(2)$ Å for R = La and $c = 10.32(5)$ Å for R = Sm. Although major peaks from the structure were clearly present, $GdAgBi_2$ powder X-ray pattern did not allow reliable refinement and estimate of lattice parameters due to small number of diffraction peaks.

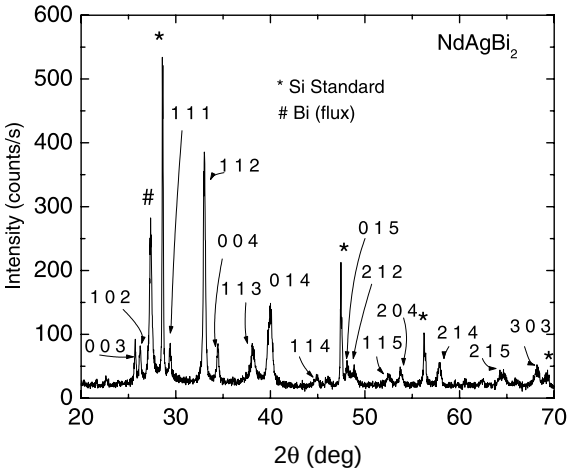

Fig. 1. Powder X-ray diffraction pattern of $NdAgBi_2$. Apart from residual Bi (#) flux and Si (*) standard, all other peaks are indexed to a tetragonal structure with $a = 4.52$ Å, $c = 10.23$ Å.

The Eu–Ag–Bi and Tb–Ag–Bi melts for various concentrations of silver up to $R_{0.045}Ag_{0.091}Bi_{0.864}$ (R = Eu, Tb) gave small crystals with cubic (R = Eu) or tetragonal (R = Tb) morphologies that were rather poorly formed. The high temperature effective moment deduced from $\chi(T)$ measurements on these crystals was not consistent with $TbAgBi_2$ and $EuAgBi_2$ stoichiometry (assuming Eu^{2+}), thus this series does not form with Eu and Tb under the same growth conditions as for the lighter rare earths.

Anisotropic field and temperature dependent magnetization measurements were made using Quantum Design MPMS-5 and MPMS-7 SQUID magnetometers in the temperature range $T = (1.8-300)$ K and in magnetic fields up to 70 kOe, applied parallel and perpendicular to the *c*-axis of the crystal. The polycrystalline average of magnetization was obtained by $\chi_{poly} = \chi_c/3 + 2\chi_a/3$. Magnetic ordering temperatures have been obtained by determination of the maximum in $\partial(\chi T)/\partial T$ and $\partial\rho/\partial T$. In plane resistance was measured using LR 400 and LR 700 AC resistance

bridges with the standard four probe method using MPMS as a H, T platform. All samples were cut into large rods for better estimates of the geometrical factor.

It should be noted that collection of the data was complicated by the problems due to air sensitivity of these materials. This leads to minor irreproducibilities when samples are cycled repeatedly. However, rare earth silver dibismites are less air sensitive than rare earth dibismites [11,18].

3. Results

Fig. 2a (inset) shows anisotropic susceptibility of $LaAgBi_2$ taken in $H = 50\,kOe$. The susceptibility is weakly temperature dependent and diamagnetic with $|\chi_a| < |\chi_c|$. For fields applied parallel to ab plane magnetic susceptibility is nearly constant, whereas c-axis susceptibility rises at lower temperatures. Whereas small concentrations of paramagnetic impurities could partially influence this rise, magnetization is also influenced by the de Haas van Alphen effect since at 50 kOe the contribution of oscillations to magnetization is positive and it rises as the temperature is decreased below 40 K (see Fig. 2b). The small break near 150 K for $H \| a$ is most likely caused by the sample movement during the measurement. Magnetic isotherms are linear in field for $H \| a$, whereas they show signs of de Haas van Alphen oscillations for $H \| c$ for $H \geqslant 20\,kOe$ and for temperatures up to at least 36 K (Figs. 2a and b). The spectrum of these oscillations is presented in the inset of Fig. 2b. Three frequencies are clearly seen, a strong peak at $F = 0.66\,MG$, and a two small peaks at $2F = 1.31\,MG$ (second harmonic of F) and $F_1 = 0.11\,MG$, which correspond to a larger and smaller pieces of Fermi surface, respectively. The temperature dependence of the amplitude can be used to determine cyclotron effective masses for a particular orbit with frequency F through the Lifshitz–Kosevitch formula for the amplitude of magnetization [19]. In order to obtain more insight into the Fermi properties of $LaAgBi_2$, we estimated effective mass for an orbit that corresponds to $F = 0.66\,MG$. Slope of $\ln(A/T)$ as a function of temperature gives $m \approx 0.07 m_0$, where m_0 is the bare electron mass, and Dingle temperature $T_D \approx 7.7\,K$. The light masses found in $LaAgBi_2$ are comparable to the ones found in $RAgSb_2$ series ($0.16-0.32 m_0$) [2].

The in-plane electrical resistivity of $LaAgBi_2$ is shown in Fig. 2c. Resistivity is metallic, linear in temperature above 100 K, and has high $RRR = (\rho(300\,K)/\rho(1.8\,K)) \sim 25$. Below 20 K, the resistivity curve is dominated by impurity scattering. No traces of superconductivity were observed down to 1.8 K. The magnetoresistance (Fig. 2c inset) is positive and substantial in size ($\Delta\rho/\rho \sim 80-120\%$). However, it is smaller in comparison with values found in rare earth silver diantimonide and rare earth dibismite series [1,11]. The apparent high temperature magnetoresistance is very likely an artifact and is caused by the progressive oxidation of the sample. For this reason, the $\rho(H)$ isotherms taken on first cool down (as in Fig. 2c inset) are more reliable, as it is the case for all magnetoresistance data in $RAgBi_2$ series. Magnetic and transport data classify $LaAgBi_2$ as a rather good metal with small anisotropy in magnetic and transport properties.

Magnetic susceptibility of $CeAgBi_2$ (Fig. 3a) is weakly anisotropic, with $\chi_a > \chi_c$ (Fig. 3a inset). The fit to polycrystalline average of χ^{-1} from 200 to 350 K gave an estimate of effective magnetic moment of Ce, $\mu_{eff} = 2.25\,\mu_B$ (close to $\mu_{eff} = 2.53\,\mu_B$ for Ce^{3+}). Using the Curie–Weiss form $\chi = C/T-$, we obtain $\theta_{poly} = 22.6\,K$, $\theta_{ab} = 31.4\,K$ and $\theta_c = 2.18\,K$. As opposed to heavier members of the series, the easy magnetization axis in low fields is the a-axis and ferromagnetic interactions are dominant along both crystalline axes. Magnetization isotherms taken at $T = 2\,K$ are shown in the second inset of Fig. 3a. For $H \| c$, two weak metamagnetic transitions are visible up to 55 kOe and induced moment values are far below the saturation value of Ce^{3+} ions. Resistivity of $CeAgBi_2$ (Fig. 3b) has $RRR \sim 15$, and below 25 K it sharply drops, probably due to the coherence in Kondo lattice and/or depopulation of crystalline field levels. Low temperature resistivity is shown in Fig. 3b inset and it shows a drop in resistivity due to the combined influence of the loss of spin disorder scattering below magnetic transition and the higher temperature contributions discussed

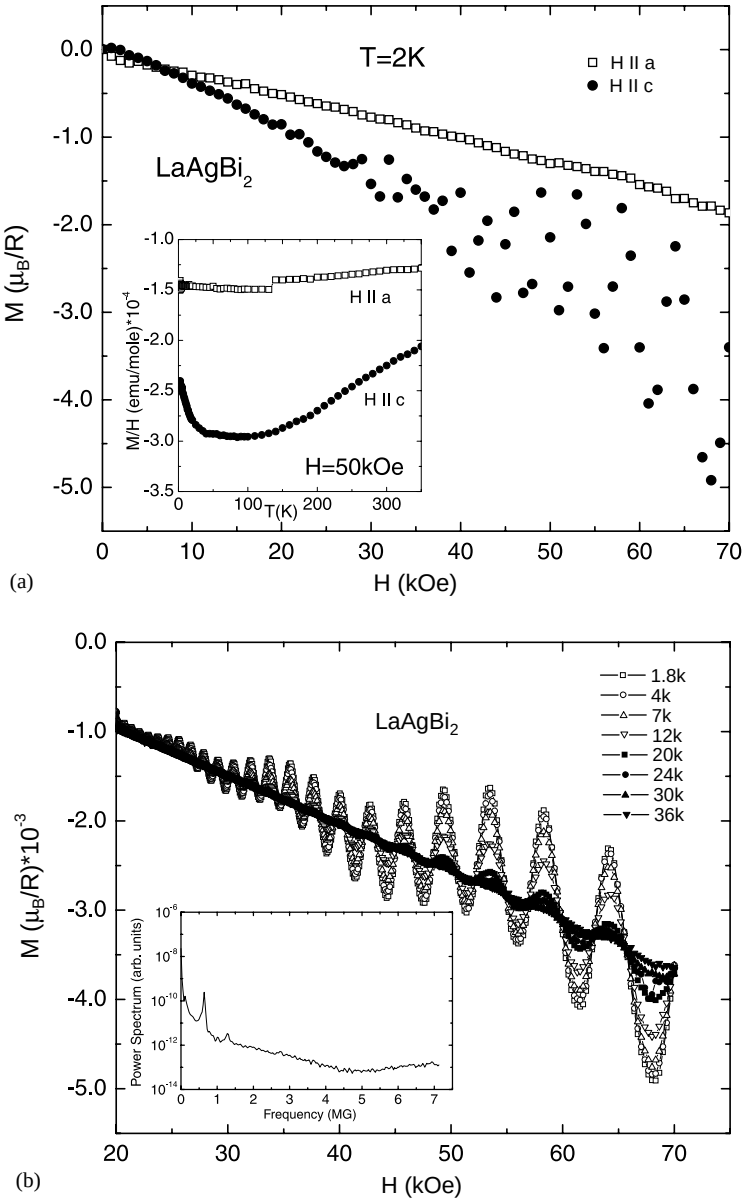

Fig. 2. (a) Magnetization isotherms of $LaAgBi_2$ as a function of magnetic field for a magnetic field applied along the c-axis (filled circles) and in the ab plane (open squares) taken at $T = 2\,K$. Inset shows temperature dependent magnetic susceptibility of $LaAgBi_2$ taken in the background field of 50 kOe. (b) De Haas van Alphen oscillations in $LaAgBi_2$ for $H \| c$ axis. Inset: spectrum of oscillations at $T = 1.8\,K$. (c) Resistivity of $LaAgBi_2$. Inset: magnetoresistance at $T = 2\,K$.

above. The magnetoresistance curves taken at $T = 2\,K$ are shown in the second inset in Fig. 3b. Magnetoresistance is linear in temperature for $H \| a$ axis, whereas for $H \| c$ it increases as $\sim H^n$ where $n = 1.25$. The apparent crossover in sign of magnetoresistance that could be inferred from main part of Fig. 3b may well be an artifact of progressive sample oxidation and would require

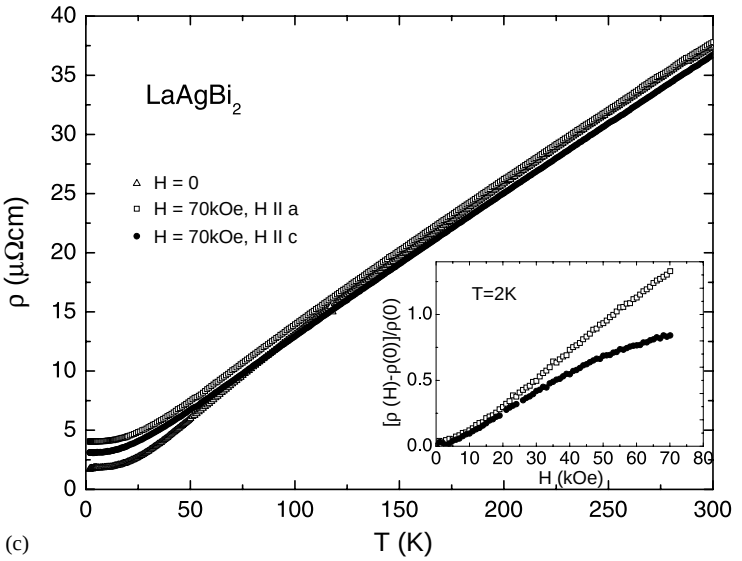

(c)

Fig. 2 (*continued*).

further measurement. From magnetization ($\partial(\chi T)/\partial T$) and resistivity ($\partial\rho/\partial T$), T_N values are 6.1 and 5.5 K. This difference is due to less reliable resistivity data due to sample oxidation as well as difficulty in separation of the loss of spin disorder scattering from coherence.

Inverse susceptibility of $PrAgBi_2$ (Fig. 4a) is linear over a rather large temperature range and the polycrystalline average at high temperatures gives the paramagnetic moment and average Curie–Weiss temperature: $\mu_{eff} = 3.56\,\mu_B$ (very close to $\mu_{eff} = 3.57\,\mu_B$ for Pr^{3+}), $\theta_{poly} = -3$ K, whereas $\theta_{ab} = 3.2$ K and $\theta_c = -17.3$ K, reminiscent of $PrBi_2$. The anisotropy in the low temperature magnetic susceptibility of $PrAgBi_2$ (Fig. 4a inset) is much smaller than in $PrBi_2$. The resistivity of $PrAgBi_2$ (Fig. 4b) has a RRR ~ 65, smaller than $PrAgSb_2$, but with similar temperature dependence. The ground state of this compound at low temperatures is likely to be nonmagnetic, but more measurements (e.g. specific heat) are needed to clarify this. Magnetization and magnetoresistance isotherms at 2 K (Fig. 4a and b insets) show weak traces of what might be a metamagnetic transition at the highest field range along the *c*-axis direction. Fields up to 70 kOe do not saturate magnetization in $PrAgBi_2$.

$NdAgBi_2$ is a well-defined local moment member of the $RAgBi_2$ series. The inverse magnetization (Fig. 5a) is linear in temperature at high temperatures, consistent with $\mu_{eff} = 3.63\,\mu_B$ (close to theoretical value of $3.61\,\mu_B$), and $\theta_{poly} = -25.1$ K. Anisotropic Weiss temperatures are $\theta_{ab} = -29.4$ K and $\theta_c = -22.3$ K. Magnetic susceptibility $\chi_{ab} > \chi_c$, but anisotropy is smaller than that seen in $NdAgSb_2$. $NdAgBi_2$ is metallic below room temperature, with RRR = 34. Resistivity (Fig. 5b) shows a drop below the magnetic ordering temperature and a broad maximum in $\partial\rho/\partial T$ at the magnetic transitions (not shown). From resistivity and magnetization measurements antiferromagnetic ordering temperatures are $T = 3.9$ K ($\partial\chi T/\partial T$) and $T = 3.8$ K ($\partial\rho/\partial T$).

The possible influence of Sm^{2+} ions and/or excitations out of the Hunds rule ground state multiplet are the likely cause of the non-Curie–Weiss magnetic susceptibility of $SmAgBi_2$ (Fig. 6a). The resistivity of this material is metallic and shows a characteristic feature of the loss of spin disorder scattering in magnetically ordered state. Magnetic isotherms taken at 2 K are linear with no sign of metamagnetic transitions. The Neel temperature values from $\partial(\chi T)/\partial T$ and

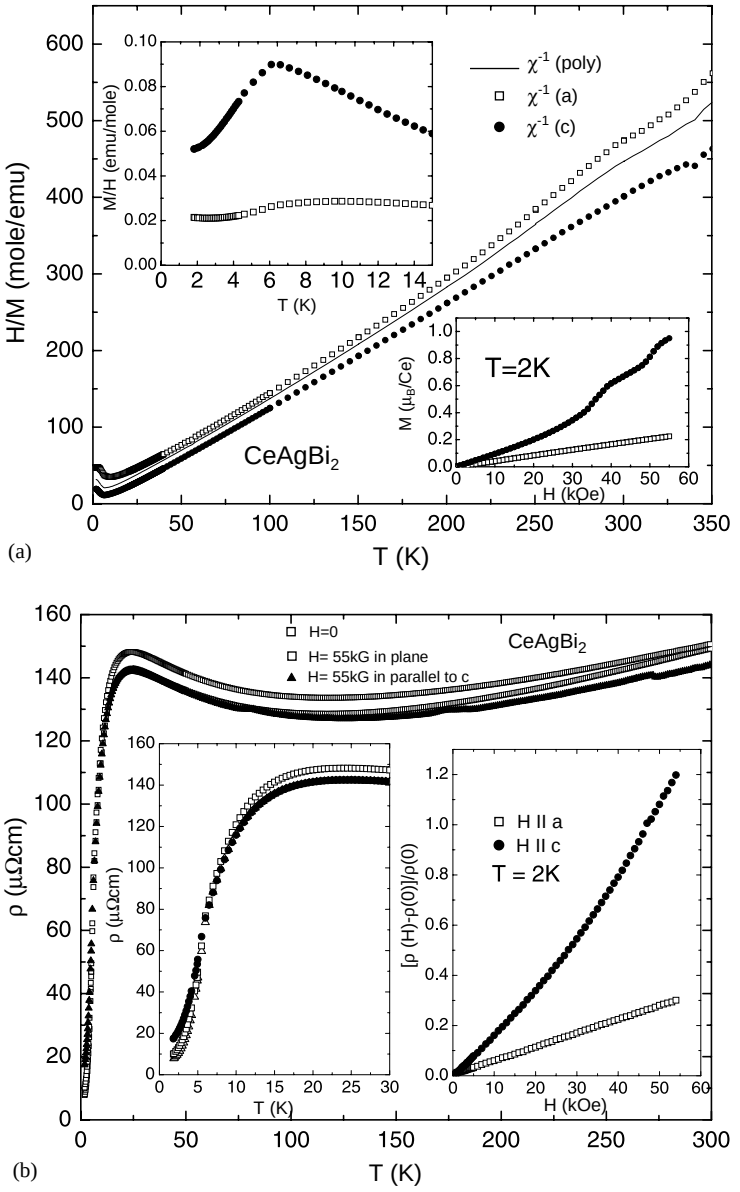

Fig. 3. (a) Temperature dependent inverse susceptibility of $CeAgBi_2$ in an applied field of $H = 1$ kOe for H along the basal plane (open squares) and along the c-axis (filled circles), and the polycrystalline average (solid line). Insets: low temperature magnetic susceptibility and magnetization isotherms taken at $T = 2$ K for $H \| a$ (open squares) and $H \| c$ (filled circles). (b) Resistivity of $CeAgBi_2$. Insets: loss of resistivity at low temperatures and magnetoresistance isotherms taken at $T = 2$ K.

$\partial\rho/\partial T$ are 8.0 K and are clearly seen in both data sets.

Fig. 7a displays the inverse susceptibility of $GdAgBi_2$. The high temperature paramagnetic moment and Weiss temperature of the polycrystalline average are $\mu_{\text{eff}} = 7.64\,\mu_B$, and $\theta_{\text{poly}} = -52$ K, close to the expected value ($\mu_{\text{eff}} = 7.93\,\mu_B$) for proposed $RAgBi_2$ stoichiometry. The Weiss paramagnetic temperatures for both crystal orientations were $\theta_a = -52$ K and $\theta_c = -55.6$ K, close to

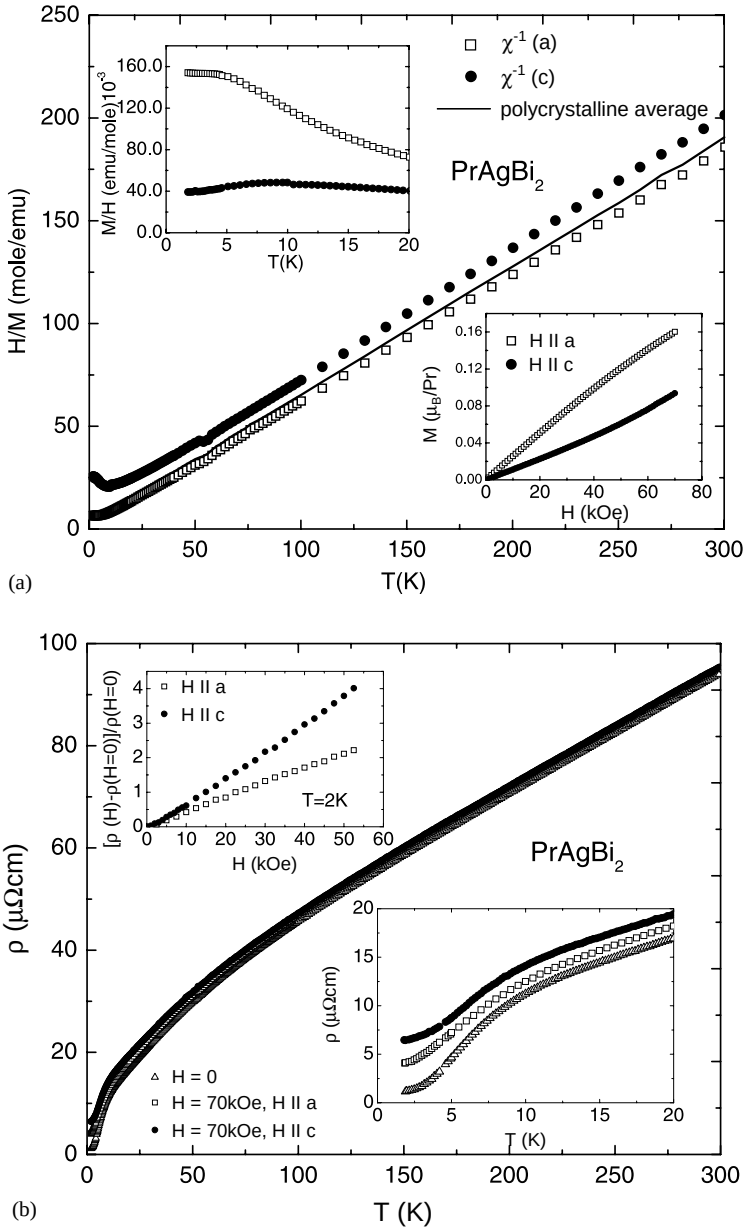

Fig. 4. (a) Inverse susceptibility of $PrAgBi_2$ for fields applied along the *c*-axis (filled circles) and the *ab* plane (open squares) taken in the background field of 1 kOe. Solid line is polycrystalline average. Insets: low temperature magnetic susceptibility of $PrAgBi_2$ and M/H isotherms taken at $T = 2\,K$. (b) Temperature dependent resistivity of $PrAgBi_2$. Insets: low temperature resistivity and magnetoresistance isotherms taken at $T = 2\,K$.

the uniform value expected for an isotropic Gd^{3+} ion with no crystal field splitting. Low temperature magnetization reveals a complex magnetic structure. In low field $H = 100\,Oe$ (Fig. 7a inset) there is a single antiferromagnetic transition and some anisotropy in the ordered state, whereas application of 10 kOe brings only a weak decrease in magnetization along the *a*-axis, followed by a

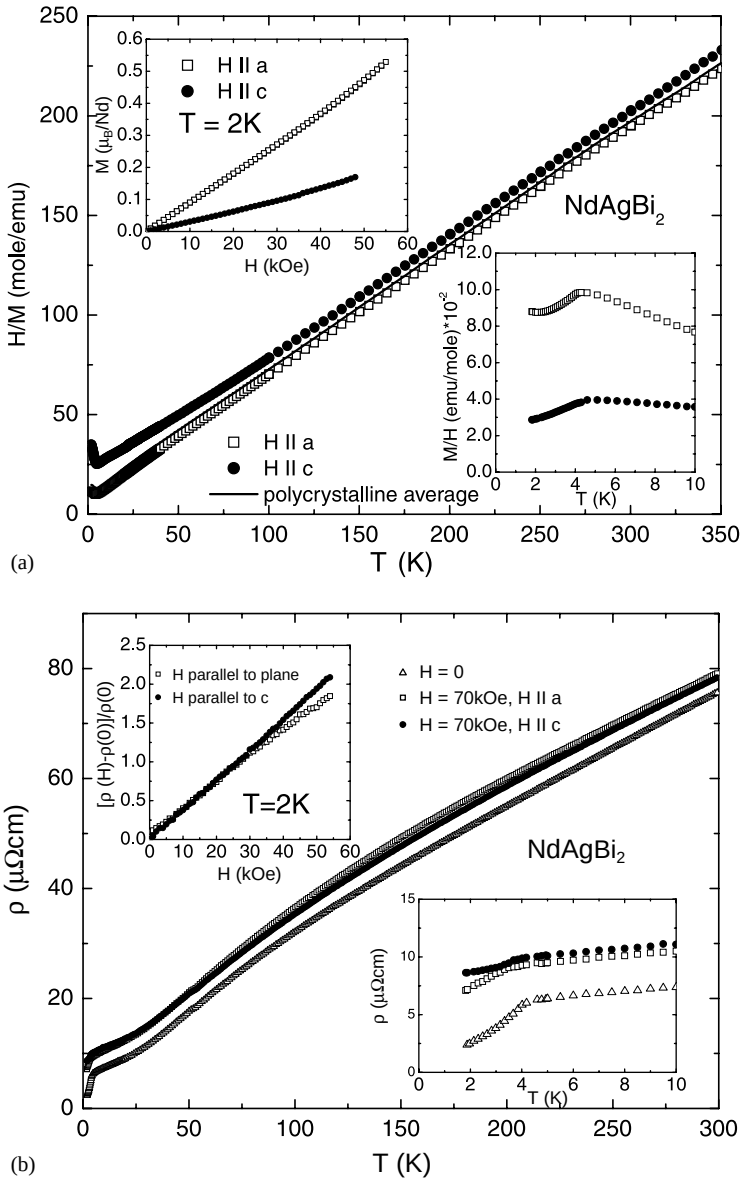

Fig. 5. (a) Inverse susceptibility of $NdAgBi_2$ as a function of temperature for a field applied along the c-axis (filled circles) and the ab plane (open squares) taken in the background field of $H = 1$ kOe. Solid line represents polycrystalline average. Insets: low temperature magnetic susceptibility and magnetization isotherms of $NdAgBi_2$ taken at $T = 2$ K. (b) Resistivity of $NdAgBi_2$. Insets: low temperature resistivity of $NdAgBi_2$ and magnetoresistance isotherms at $T = 2$ K.

small increase which smears out the anisotropy. Magnetic isotherms (Fig. 7a inset) taken at 2 K with 1000 Oe steps are linear in field and still far away from the saturation value of Gd^{3+} moments. Spin reorientation, rather than population of higher crystal field levels is the likely cause of increased a-axis susceptibility in the ordered state of $GdAgBi_2$. The resistivity of $GdAgBi_2$ is shown in Fig. 7b. The RRR ~ 2.5 is markedly smaller than in the case of lighter rare earths. Together with the discrepancy in high temperature paramagnetic moment, it points to defects and disorder

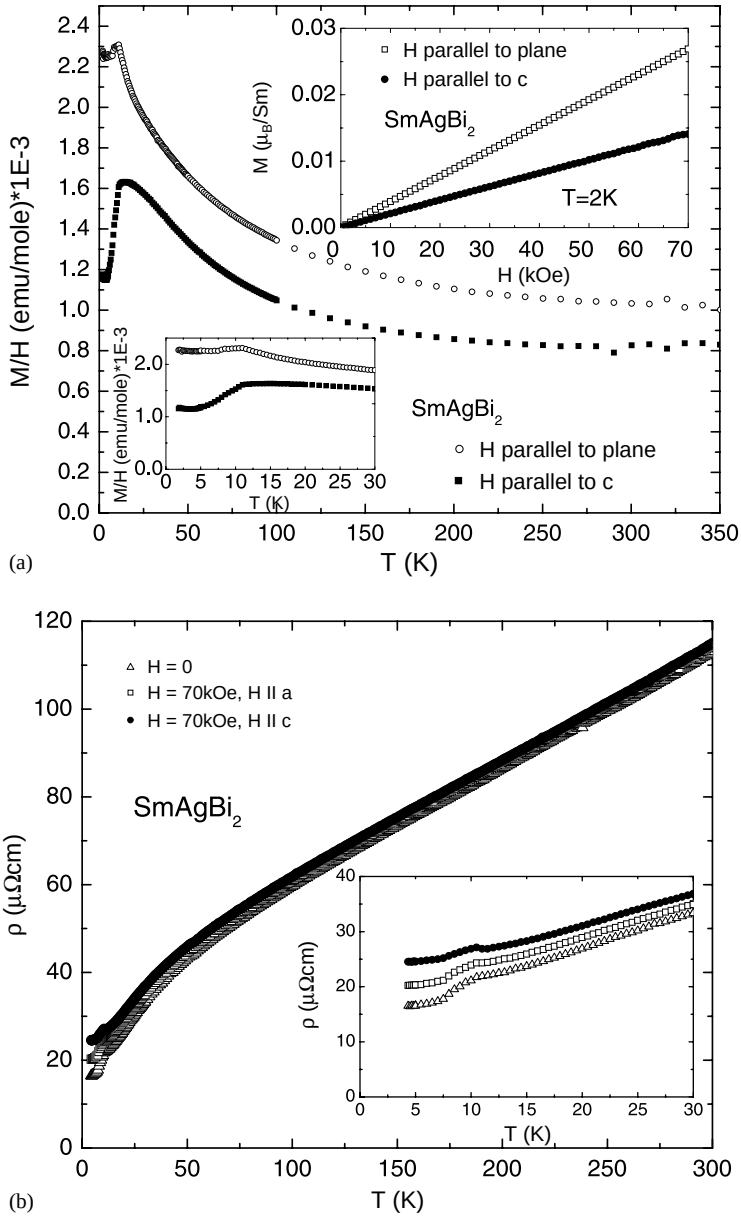

Fig. 6. (a) Magnetic susceptibility of $SmAgBi_2$ as a function of temperature for a field applied along the *c*-axis (filled circles) and the *ab* plane (open squares) taken in $H = 1$ kOe. Insets: low temperature magnetic susceptibility and magnetization isotherms at $T = 2$ K. (b) Resistivity of $SmAgBi_2$. Insets: low temperature resistivity.

in the crystal structure. Low temperature resistivity shows loss of spin disorder scattering below Neel temperature and magnetoresistance isotherms taken at 2 K show no sign of metamagnetism. However, in the low field below 1000 Oe both magnetic and magnetoresistance isotherms should show feature associated with metamagnetic transition shown in the inset of Fig. 7a (inset).

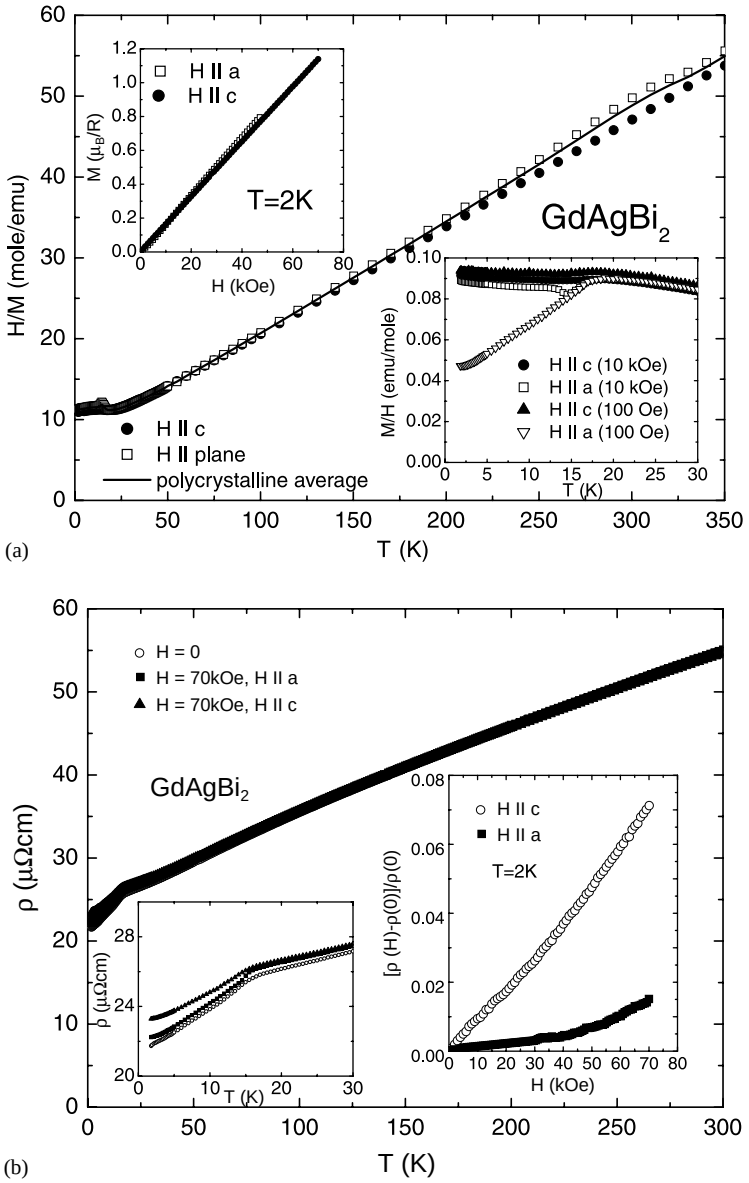

Fig. 7. (a) Temperature dependent inverse susceptibility of $GdAgBi_2$ in an applied field of $H = 10\,\text{kOe}$ for $H \| c$ (filled circles) and $H \| a$ axis (open squares). Insets: low temperature susceptibility and magnetization isotherms taken at $T = 2\,\text{K}$. (b) Temperature dependent resistivity of $GdAgBi_2$. Note substantial decrease in RRR when compared to $LaAgBi_2$. Insets: low temperature resistivity and magnetoresistance isotherms taken at $T = 2\,\text{K}$.

4. Discussion and conclusions

$LaAgBi_2$ is an interesting example of a rare earth intermetallic compound with a rather low effective mass of its electronic system. All $RAgSb_2$ compounds order antiferromagnetically, except non-Kramers $PrAgBi_2$. The high temperature magnetic behavior of the Ce, Pr, Nd and Gd members of the $RAgBi_2$ series is local moment-like and the values of the effective magnetic moment in

the paramagnetic state are close to the theoretical values. The Curie–Weiss temperature θ_{poly} changes monotonically from $PrAgBi_2$ to $GdAgBi_2$ (with the exception of non-Curie–Weiss $SmAgBi_2$). The lack of scaling in the case of $CeAgBi_2$ is likely due to hybridization of the 4f Ce levels.

There is a poor scaling of Neel ordering temperatures with the de Gennes factor $DG = [(g_J - 1)^2 J(J+1)]$, where the Lande g-factor is defined as $g_J = 3/2 + \{[S(S+1) - L(L+1)]/J(J+1)\}$ (Fig. 8). In the indirect exchange model of Rudermann–Kittel–Kasuya–Yosida (RKKY), magnetic ordering temperature T_N is proportional to DG: $T_N \sim 8N(E_F)k_B I^2\,DG$, where $N(E_F)$ is the density of states at the Fermi level, k_B is the Boltzman constant, and I is the exchange parameter. The influence of crystal fields can be responsible for a breakdown of scaling of the ordering temperatures.

The dominant interactions along both crystalline axes for $CeAgBi_2$ are ferromagnetic. However, $CeAgBi_2$ seems to order antiferromagnetically in the background of $H = 1$ kOe, in contrast to the isostructural Ce-based Kondo lattice system $CeAgSb_2$ [1]. The low temperature magnetoresistance found in rare earth silver dibismites was positive, close to linear, and with similar values of anisotropy as it was found in $RAgBi_2$ [1]. It is not as large in magnitude as in $RAgSb_2$, although

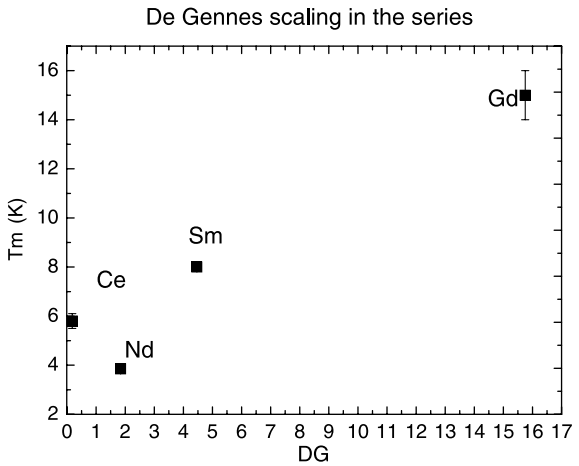

Fig. 8. De Gennes scaling of the magnetic ordering temperatures in the series.

light members of the series had low residual $\rho_0 \sim 10^{-6}\,\Omega$ cm and large RRR values. Since the magnitude of magnetoresistance in $RAgBi_2$ compounds scales with the magnitude of RRR (see for example $PrAgBi_2$ and $GdAgBi_2$), we conclude that conduction electron relaxation times decrease strongly due to structure imperfections with the increase of the mass of rare earth ion. The Fermi surface characteristics are necessary for the exact analysis of magnetoresistance in $RAgBi_2$. A thorough and thoughtful review of possible mechanisms can be found in Ref. [6].

5. Summary

We have successfully synthesized a new series of rare earth compounds, $RAgBi_2$ (R = La–Nd, Sm, Gd), and delineated their basic structural, magnetic and electronic transport properties utilizing single crystals made via self-flux method. This further expands the range of formation of the $ZrCuSi_2$ structure type into R–Ag–Bi ternary solutions. $LaAgBi_2$ is a diamagnet with an effective electronic mass as small as $0.07m_0$ for some of the Fermi surface sheets. All other rare earth silver dibismites exhibit metallic antiferromagnetism except non-Kramers $PrAgBi_2$. This material is likely to be nonmagnetic above 1.8 K, but further measurements are necessary to clarify this. The RKKY model fails to explain magnetic ordering temperatures in the series due to the effect of crystal fields or differences in the electronic structure with varying rare earth ions. When compared to isostructural $RAgSb_2$ or closely related RSb_2 and RBi_2, the $RAgBi_2$ compounds show less anisotropy in their magnetic properties and less transverse magnetoresistance. Based on resistivity measurements and high values of magnetic susceptibility at low temperatures, $CeAgBi_2$ is likely to have significant hybridization between 4f and the conduction band. Specific heat measurements are desirable to get further insight into possible heavy fermion characteristics of this ternary rare earth intermetallic compound that stand in sharp contrast to the

extremely light effective mass of carriers in isostructural $LaAgBi_2$.

Acknowledgements

We thank W. Choe and G. Miller for fruitful discussions. Ames Laboratory is operated for the US Department of Energy by Iowa State University under contract No. W-7405-Eng. 892. This work was supported by the Director for Energy Research, Office of Basic Energy Sciences.

References

[1] K.D. Myers, S.L. Bud'ko, I.R. Fisher, Z. Islam, H. Kleinke, A.H. Lacerda, P.C. Canfield, J. Magn. Magn. Mater. 205 (1999) 27.
[2] K.D. Myers, S.L. Bud'ko, V.P. Antropov, B.N. Harmon, P.C. Canfield, A.H. Lacerda, Phys. Rev. B 60 (1999) 13371.
[3] J.A. Dann, A.D. Hillier, J.G.M. Armitage, R. Cywinski, Physica B 289–290 (2000) 38.
[4] M.J. Thornton, J.G.M. Armitage, G.J. Tomka, P.C. Riedi, R.H. Mitchell, M. Houshiar, D.T. Adroja, B.D. Rainford, D. Fort, J. Phys. Condens. Matter 10 (1998) 9485.
[5] G. Andre, F. Bourée, M. Kolenda, B. Leśniewska, A. Oleś, A. Szytuła, Physica B 292 (2000) 176.
[6] S.L. Bud'ko, P.C. Canfield, C.H. Mielke, A.H. Lacerda, Phys. Rev. B 57 (1998) 13624.
[7] T. Kagayama, G. Oomi, S.L. Bud'ko, P.C. Canfield, Physica B 281–282 (2000) 90.
[8] A. Kagawa, T. Kagayama, G. Oomi, H. Mitamura, T. Goto, P.C. Canfield, S.L. Bud'ko, Physica B 281-282 (2000) 124.
[9] J.C.H. Mielke, N. Harrison, A.H. Lacerda, S.L. Bud'ko, P.C. Canfield, J. Phys.: Condens. Matter 10 (24) (1998) 5289.
[10] K.D. Myers, P.C. Canfield, V.A. Kalatsky, V.L. Pokrovsky, Phys. Rev. B 59 (1999) 1121.
[11] C. Petrovic, S.L. Bud'ko, P.C. Canfield, J. Magn. Magn. Mater. 247 (2002) 270.
[12] Z. Fisk, J.P. Remeika, in: K.A. Gschneider, J. Eyring (Eds.), Handbook on the Physics and Chemistry of Rare Earths, Vol. 12, Elsevier, Amsterdam, 1989.
[13] P.C. Canfield, Z. Fisk. Phil. Mag. B 65 (1992) 1117.
[14] P.C. Canfield, I.R. Fisher, J. Cryst. Growth 225 (2–4) (2001) 155.
[15] M. Brylak, M. Möller, W. Jeitschko, J. Solid State Chem. 115 (1995) 305.
[16] H. Flandorfer, O. Sologub, C. Godart, K. Hiebl, A. Leithe-Jasper, P. Rogl, H. Noël, Solid State Commun. 97 (1996) 305.
[17] Y. Muro, N. Takeda, M. Ishikawa, J. Alloys Compounds 257 (1997) 23.
[18] K. Yoshinara, J.B. Taylor, L.D. Calvert, J.G. Despault, J. Less-Common Met. 41 (1975) 329.
[19] D. Shoenberg, Magnetic Oscillations in Metals, Cambridge University Press, Cambridge, England, 1984.